

Quantum network of neutral atom clocks

P. Kómár,¹ T. Topcu,^{1,2,3} E. M. Kessler,^{1,3} A. Derevianko,^{1,2,3} V. Vuletić,⁴ J. Ye,⁵ and M. D. Lukin¹

¹*Physics Department, Harvard University, Cambridge, MA 02138, USA*

²*Department of Physics, University of Nevada, Reno, NV 89557, USA*

³*ITAMP, Harvard-Smithsonian Center for Astrophysics, Cambridge, MA 02138, USA*

⁴*Department of Physics and Research Laboratory of Electronics,
Massachusetts Institute of Technology, Cambridge, MA 02139, USA*

⁵*JILA, NIST, Department of Physics, University of Colorado, Boulder, CO 80309, USA*

(Dated: March 22, 2016)

We propose a protocol for creating a fully entangled GHZ-type state of neutral atoms in spatially separated optical atomic clocks. In our scheme, local operations make use of the strong dipole-dipole interaction between Rydberg excitations, which give rise to fast and reliable quantum operations involving all atoms in the ensemble. The necessary entanglement between distant ensembles is mediated by single-photon quantum channels and collectively enhanced light-matter couplings. These techniques can be used to create the recently proposed quantum clock network based on neutral atom optical clocks. We specifically analyze a possible realization of this scheme using neutral Yb ensembles.

PACS numbers: 03.67.Ac, 03.67.Bg 32.80.Rm

The current record in clock accuracy is held by ytterbium and strontium clocks [1], capable of reaching $\sim 10^{-18}$ fractional frequency stability [2, 3]. Apart from the enormous amount of effort and innovation, the unprecedented precision and accuracy were attainable due to the large number of clock atoms ($10^3 - 10^4$) [4]. Super-stable clocks enable evaluation of the systematic frequency shift of atomic transitions with less averaging time, which is important to measure fast transients, e.g. gravitational waves and passing dark-matter clumps [5]. In our recent work [6], we showed that a quantum network of atomic clocks can result in substantial boost of the overall precision if multiple clocks are connected in quantum entanglement. The proposed globally entangled state, Greenberger-Horne-Zeilinger (GHZ) state, is more sensitive to the global phase evolution of the clock atoms, thus allows for an improved measurement of the passage of time. If the GHZ state is set up and interrogated in the optimal way [7, 8], frequency measurements can asymptotically reach the Heisenberg limit [9], associated with the total number of atoms in the entire network. Significant noise reduction has recently been demonstrated with spin-squeezed states in a single ensemble of atoms [10]. Efforts are being made to make both the non-local [11] and local entanglement distribution [12, 13] faster and more reliable. Of particular interest are applications of these ideas to neutral atom clocks.

In this Letter, we show how a non-local GHZ state can be created across multiple, spatially separated neutral atom clocks with high fidelity. Our protocol relies on strong Rydberg blockade for enhancing local atom-atom interaction, collective excitations for enhancing photon-atom interaction, and single photon quantum channels for reliable remote connections. We propose and analyze a realization using neutral Yb ensembles, suitable for the current atomic clock technology. We predict that thousands of atoms can be entangled to give an overall

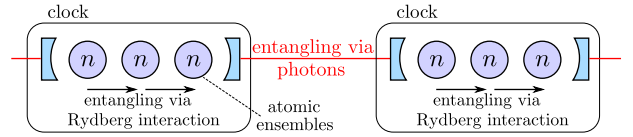


FIG. 1. (Color online) Schematic of the setup. K clocks, each holding M atomic ensembles of size n are connected. Atoms within each ensemble get entangled using long-range interaction between Rydberg atoms, ensembles in the same clock are entangled either via Rydberg interactions or via the cavity mode, while neighboring clocks are entangled through single-photon quantum channels, enhanced by optical cavities. The resulting state is a global GHZ state, $|0\rangle^{\otimes N} + |1\rangle^{\otimes N}$ of all $N = KMn$ atoms in the network.

stability increase of more than an order of magnitude, compared to non-entangled clock networks. We emphasize that our protocol, although presented to be used for a network, can also be applied to a single ensemble.

We describe our protocol for K identical atomic clocks arranged in a sequence, each connected to its neighbors with optical channels, and each using Mn identical atoms, trapped in a magic-wavelength optical lattice, distributed in M ensembles, illustrated on Fig. 1. We use the atomic levels, shown on Fig. 2(a) for our protocol: The two levels of the clock transition, g, f , a metastable shelving level s , an excited level e , which spontaneously decays to g , and two strongly interacting Rydberg levels, r_1 and r_2 . We further require transitions between levels, marked with arrows, to be driven independently.

We imagine preparing all atoms in the ground state g , after which our protocol consists of five subsequent steps. First, using blockade, we create two independent collective excitations in one ensemble in each clock, using two separate atomic levels (f and s). Second, each excited ensemble emits single photon pulses that are entangled with one of these collective excitations. Third, the pho-

tons are sent towards the neighboring atomic clocks, and measured with a linear optics setup in Bell-basis. Fourth, upon success, each clock performs a local CNOT operation to connect the two collective excitations. The result is a set of K entangled collective excitations, one in the first ensemble of each clock, which serve as "seeds" for a global GHZ state. In the fifth, and final, step the clocks locally "grow" a GHZ state out of each seed, extending it to all atoms in the clock, and thus a global GHZ state is obtained. In the following, we provide detailed description and analysis of these five steps, discuss the specific realization in Yb atoms and analyze the most important sources of imperfections and errors.

Our scheme makes use of the Rydberg blockade, which is a result of the interaction arising between atoms excited to Rydberg states in an ensemble. If driven resonantly, the first excited atom blocks the transition of a second one, thus at most one atom can get coherently excited to the Rydberg state [14–16], allowing precise quantum control. Rydberg blockade has been proposed as an efficient tool to realize quantum gates and perform quantum information processing [13, 17–21]. Efficient control requires the atoms to reside within the blockade radius of the Rydberg atom. Different ways of trapping and manipulating Rydberg states are currently under investigation both experimentally [22–26] and theoretically [27–29].

In the first step, we make use of the Rydberg blockade to create a superposition of one and zero excitation in both f and s levels, following the approach of [13, 14, 17]. This is done by performing the following sequence of driving pulses: $[\pi/(2\sqrt{n})]_{g,r1}$, $[\pi]_{f,r1}$, $[\pi]_{f,s}$, $[(\pi/(2\sqrt{n}))]_{g,r1}$, $[\pi]_{f,r1}$, shown in Fig. 2(a), where $[\phi]_{a,b}$ stands for a pulse with total, single-atom Rabi phase ϕ between level a and b . Starting from the state $|g\rangle^{\otimes n} =: |0\rangle$, this pulse sequence creates the state

$$(1 + f^\dagger)(1 + s^\dagger)|0\rangle =: (|0_f\rangle + |1_f\rangle)(|0_s\rangle + |1_s\rangle), \quad (1)$$

where f^\dagger and s^\dagger are creation operators of the two (approximately) independent spin wave modes, supported by the two levels f and s .

In the second step, spin-photon entangled states, using the spin wave modes f and s , are created, based on an extended version of the scheme described in [30] and collective enhancement. Each spin-photon entangled state is created by the pulse sequence shown in Fig. 2(b), involving $[\pi]_{s,r2}$, $[\pi/\sqrt{n}]_{g,r1}$, $[\pi]_{e,r1}$, $[\pi]_{s,r2}$. With additional pulses applied before and after this sequence flipping between $0_f \leftrightarrow 1_f$, $0_s \leftrightarrow 1_s$ and swapping f and s waves, and proper timing, this is repeated four times to produce four time-bin separated light pulses, which are entangled with the two spin waves,

$$(|0_f\rangle|t_2\rangle + |1_f\rangle|t_4\rangle)(|0_s\rangle|t_1\rangle + |1_s\rangle|t_3\rangle), \quad (2)$$

where $|t_j\rangle|t_k\rangle$ is a two photon state with photons emitted at times t_j and t_k .

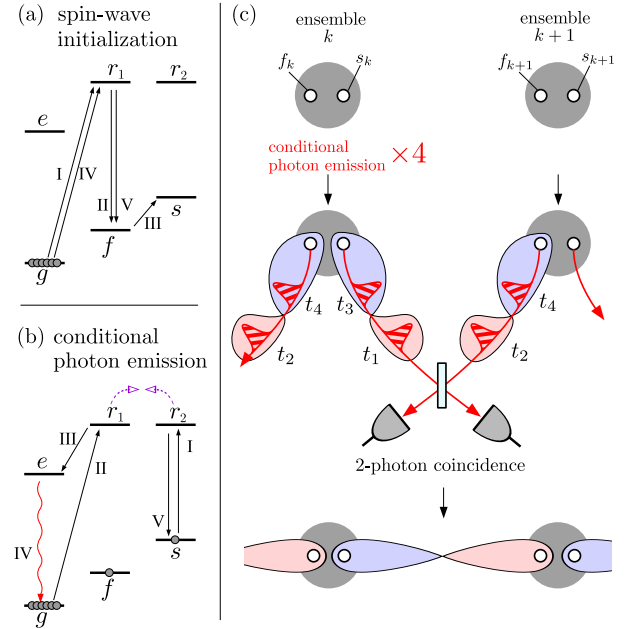


FIG. 2. (Color online) Steps to generate pairwise entanglement. (a) Pulse sequence used to initialize the spin-waves f and s in an ensemble. (b) Pulse sequence inducing a conditional photon emission, the emitted photon becomes entangled with the spin state s . (c) In three steps, neighboring ensembles generate pairwise entanglement between their collective excitations. First, they induce $0 + 1$ superpositions of the two independent spin waves, f^\dagger and s^\dagger . Then applying the conditional photon emission sequence four times, they emit four pulses, containing two photons total. Each pair of photons is correlated with a unique spin state. Finally, photons are measured with a linear optics setup, and 2-photon coincidences indicate the creation of entanglement between neighboring ensembles. (Blue and red shadings indicate positive and negative correlation between qubits, respectively.)

In the third step, pairs of time-bin encoded photon pulses from two neighboring ensembles are detected by interfering the two pulses on a beam splitter and measuring two-photon coincidences [31–33]. As a result, entangled states between neighboring atomic ensembles, k and $k + 1$, are created [34, 35],

$$|0_s\rangle_k |1_f\rangle_{k+1} \pm |1_s\rangle_k |0_f\rangle_{k+1}, \quad (3)$$

where the individual kets represent the states of f and s spin waves in the two ensembles, see Fig. 2(c).

In the fourth step, the ensembles perform a local CNOT operation on the two collective degrees of freedom, f^\dagger and s^\dagger . This is done with the following pulse sequence, $[\pi]_{s,r2}$, $[\pi]_{f,r1}$, $[\pi/\sqrt{n}]_{g,r1}$, $[\pi]_{f,r1}$, $[\pi]_{s,r2}$, shown on Fig. 3(a), which promotes any population in s to r_2 , which then blocks the path through r_1 . The result is a conditional flip $|0_f\rangle \leftrightarrow |1_f\rangle$, conditioned on having zero s^\dagger excitations. If we perform $f \leftrightarrow s$ swaps before and after this process, we get a coherent flip between $|0_f, 0_s\rangle \leftrightarrow |0_f, 1_s\rangle$.

To understand the resulting state, let us consider two

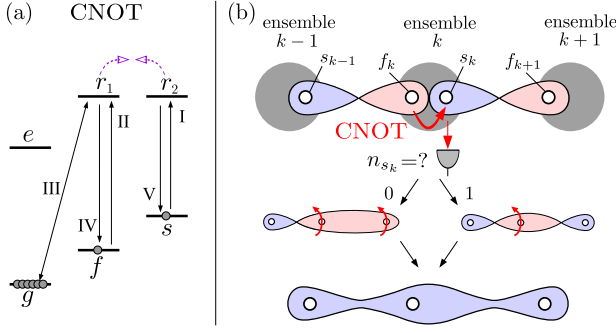


FIG. 3. (Color online) Connecting links into non-local GHZ state. (a) CNOT gate between the two excitations f and s : If level s is occupied, then the coherent (de)excitation of the f level is blocked by the Rydberg blockade between the r_1 and r_2 intermediate levels, otherwise it succeeds. (b) Connecting two entanglement links. The local CNOT and measurement operations on ensemble k entangle the two, initially independent, parts of the system: s_{k-1}, f_k and s_k, f_{k+1} . Depending on the outcome of the measurement, either only f_k , or the entire right hand side needs to be flipped, in order to arrive to the proper GHZ state.

entangled links, connecting three neighboring ensembles $k-1, k$ and $k+1$ as shown in Fig. 3(b). The corresponding state, before the fourth step, is

$$(|0, 1\rangle + |1, 0\rangle)_{s_{k-1}, f_k} \otimes (|0, 1\rangle + |1, 0\rangle)_{s_k, f_{k+1}}, \quad (4)$$

where $|n_{s_{k-1}}, n_{f_k}\rangle \otimes |n_{s_k}, n_{f_{k+1}}\rangle$ indicate the number of excitations in the modes $s_{k-1}, f_k, s_k, f_{k+1}$ of the three ensembles. After the conditional flip of s_k and measurement of $n_{s_k} \rightarrow m \in \{0, 1\}$, the state becomes $|0, 1, 1-m\rangle + |1, 0, m\rangle$, where the remaining kets stand for $|n_{s_{k-1}}, n_{f_k}, n_{f_{k+1}}\rangle$. Depending on the outcome, either only f_k (if $n_{s_k} \rightarrow 1$) or the entire right hand side (if $n_{s_k} \rightarrow 0$) needs to be flipped in order to obtain the desired GHZ state, $\bigotimes_k |0_f\rangle_k + \bigotimes_k |1_f\rangle_k$, of the f excitations of each clock, $k = 1, 2, \dots, K$.

In the fifth step, each clock locally extends the entanglement from its f degree of freedom to all atoms using a collective Rydberg gate similar to the ones introduced in Refs. [36, 37]. In the case when each clock consists of a single blockaded ensemble, the pulse sequence $[\pi]_{f,s}, [\pi/2]_{s,r2}, ([\pi/\sqrt{n-j+1}]_{g,r1}, [\pi/\sqrt{j}]_{f,r1} \text{ for } j = 1, 2, \dots, n), [\pi]_{s,r2}$, shown in Fig. 4(a), does exactly that. This sequence transfers the atoms one by one from g to f only if r_2 is unoccupied, and gets blocked otherwise. The result is

$$\bigotimes_{k=1}^K |0_f\rangle_k + \bigotimes_{k=1}^K |1_f\rangle_k \rightarrow \bigotimes_{k=1}^K |f\rangle^{\otimes n} + \bigotimes_{k=1}^K s^\dagger |g\rangle^{\otimes n}, \quad (5)$$

where $|f\rangle$ and $|g\rangle$ denote the state of a single atom. Finally, we get rid of the s excitation with a series of pulses that move it back to g : $[\pi]_{f,s}, [\pi]_{f,r1}, [\pi]_{f,s}, [\pi/\sqrt{n}]_{g,r1}$, and end up with $|f\rangle^{\otimes Kn} + |g\rangle^{\otimes Kn}$, a fully entangled state of all $N = Kn$ atoms in the network.

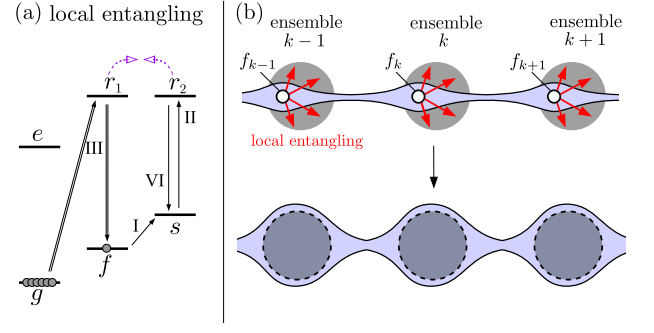


FIG. 4. (Color online) Local GHZ creation. (a) Conditional, local GHZ state generation: Any excitation in level s prevents the transfer from g to f . (b) The local entangling operation extends the GHZ state from the f spin-wave to all atoms. As a result, every atom in the network gets entangled.

In practice, lattice clocks can employ $n = 10^3 - 10^4$ atoms each, that can not be manipulated simultaneously with high fidelity using Rydberg blockade (see discussion below). In such a case, the atoms can be separated into $M \sim 10$ ensembles within each clock, as shown in Figure 1. Efficient local entanglement can be achieved with techniques described in [38] or by using an individually addressed “messenger” atom, that can be moved to the vicinity of each ensemble to entangle all atoms within each clock using dipole-dipole interaction. In such a case, the messenger atom can be used, first, to extend the entanglement to all ensembles in each clock, resulting in a state $|1_f\rangle^{KM} + |0\rangle^{KM}$, after which the procedure shown in Fig. 4(a) applied within each ensemble can be used to a fully entangled state of all $N = K \times Mn$ atoms in the network. (See Supplementary for details.)

Next, we investigate the robustness of our protocol in light of realistic physical imperfections. We assume that all imperfections decrease the coherence between the two components of the GHZ state, and therefore the fidelity can be written as $F = [1 + \exp(-\varepsilon_{\text{tot}})]/2$, where ε_{tot} is the sum of the errors. The errors arising during each non-local connection step $\varepsilon_{\text{non-local}}$ and the errors arising during a local GHZ creation in one clock $\varepsilon_{\text{local}}$ add up to the total error

$$\varepsilon_{\text{tot}} = (K-1)\varepsilon_{\text{non-local}} + KM\varepsilon_{\text{local}}. \quad (6)$$

This error increases linearly with the total number of atoms in the network, N , and the coefficient, $(\varepsilon_{\text{non-local}}/M + \varepsilon_{\text{local}})/n$, depends on the number of atoms, n , within a single atom cloud under blockade. For a certain optimal local atom number n_{opt} , the total fidelity is maximal, i.e. decreases with the slowest rate, as N increases.

To be specific, we focus on a possible implementation of our scheme with ensembles of neutral ytterbium atoms whose relevant electronic levels are shown on Fig. 5. We identify the following levels of neutral Yb relevant for our protocol: $|g\rangle = |6s^2(^1S_0)\rangle$, $|f\rangle = |6s6p(^3P_0)\rangle$, $|s\rangle = |6s6p(^3P_2)\rangle$ and $|e\rangle = |6s6p(^1P_1)\rangle$, and two Rydberg

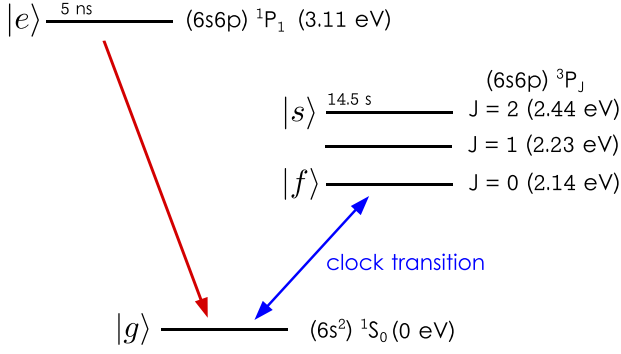


FIG. 5. (Color online) Implementation of our protocol in the lower level of neutral Yb. We assign the roles of g and f to the clock levels, the role of s to the metastable $J = 2$ level of $6s6p$, and the role of e to the 1P_1 excited state, which spontaneously decays to the ground state.

levels $|r_1\rangle = |6s\tilde{n}p_{m=+1}(^1P_1)\rangle$ and $|r_2\rangle = |6s\tilde{n}s(^3S_1)\rangle$ with the same principle quantum number \tilde{n} . Collective enhancement and phase matching of the laser pulses make the emitted photons leave in a well-defined, narrow solid angle, resulting in high photon collection efficiency. Due to the different symmetries of these states, the coherent coupling can be done via 1-photon transitions for $r_1 \leftrightarrow g$ and $r_2 \leftrightarrow s$, and requires 2-photon transitions for $r_1 \leftrightarrow e$ and $r_1 \leftrightarrow f$. We envision the atoms being held in position by an optical lattice with period $a = 275.75$ nm, each potential minimum holding exactly one Yb atom. (The lattice intensity can be modulated during the Rydberg state excitation [39].)

We consider the following errors in our analysis. During non-local connection, we take into account the finite r_1 - r_2 interaction, which allows the creation of an r_1 excitation with some small probability, even if r_2 is populated, the finite lifetime of the s and r_2 levels, and the dark-count rate of photo-detectors. For the local GHZ creation step, we account for the same imperfection of the r_1 - r_2 blockade as for the non-local entangling step, the finite lifetimes of the Rydberg levels r_1 and r_2 , and the imperfect self-blockade of the single excited Rydberg states r_1 . (See Supplementary Materials for details.) We estimate the effect of these errors, and numerically optimize the free parameters: the Rabi frequency Ω of the transferring pulses $g \rightarrow r_1$ and $r_1 \rightarrow f$, and the number of local atoms n , for principle quantum numbers, $50 \leq \tilde{n} \leq 150$ of the Rydberg levels, in order to find the minimal error per atom, $E := \varepsilon_{\text{tot}}/N$.

To illustrate, for Rydberg levels $\tilde{n} = 120$, we find that the highest fidelity is reached for $n_{\text{opt}} \approx 146$, and $\Omega = 10^5 \gamma$, where $\gamma \sim 10^3 \text{ s}^{-1}$ is the natural linewidth of the Rydberg levels, for a clock size of $(Mn)_{\text{opt}} = 2500$. In this case, the error per atom is $E_{\text{min}} = [\varepsilon_{\text{tot}}/N]_{\text{min}} = 1.8 \times 10^{-5}$. Contributions of the different error sources are shown in Table I. We find that the decay of the Rydberg level, and imperfect blockade cause the majority of imperfections, both arising during the critical step, local

Errors in 3D ensemble	error per atom	ratio in total
imperfect blockade (e_1)	2.6×10^{-6}	14%
Rydberg decay (e_2)	1.6×10^{-5}	86%
self-blockade (e_3)	$\sim 10^{-11}$	< 0.1%
r_2 decay (non-local) (e_4)	$\sim 10^{-11}$	< 0.1%
photon detection (e_5)	$\sim 10^{-12}$	< 0.1%
memory error (e_6)	$\sim 10^{-8}$	< 0.1%
photon collection (e_7)	$\sim 10^{-8}$	< 0.1%
total error per atom	1.8×10^{-5}	100%

TABLE I. The absolute and relative contribution of the different error sources to the total error per atom E , at $\tilde{n} = 120$, $\Omega = \Omega_{\text{opt}} = 10^5 \gamma$ and $n = n_{\text{opt}} = 146$, after numerical optimization, for a 3D lattice. (See Supplementary Materials for 2D results.)

extension of the GHZ state. (See Supplementary Materials for more details.)

With the optimal ensemble size n_{opt} , determined above, we consider the total number of entangled atoms N . Although having more atoms always results in improved clock precision, entangling all available atoms is not necessarily optimal. To see this, we compare the stability of the entangled clock network and a non-entangled network, and find an optimal entangled atom number N_{opt} by maximizing the stability gain over the non-entangled scheme,

$$G = \frac{\sigma_{\text{non-ent}}}{\sigma_{\text{ent}}/(2F-1)} = e^{-EN} \frac{\pi}{8} \sqrt{\frac{N}{\log N}}, \quad (7)$$

where $\sigma_{\text{ent}} = \frac{1}{\omega_0 \tau \pi} \frac{8 \sqrt{\log N}}{N}$ (from [6], assuming perfect fidelity, and that τ is smaller than the reduced atomic coherence time $\gamma_{\text{at}}^{-1}/N$) and $\sigma_{\text{non-ent}} = \frac{1}{\omega_0 \tau} \frac{1}{\sqrt{N}}$ (for N independent atoms) are the Allan deviations of the two schemes, where ω_0 is the central frequency and τ is the total available measurement time. The additional factor of $2F-1 = e^{-EN}$ is due to the reduced Fisher information of a non-pure GHZ state, where F is the fidelity of the initial state. (See supplementary materials for details.) For $E = E_{\text{min}} = 1.8 \times 10^{-5}$, Eq. (7) is maximized with optimal atom number $N_{\text{opt}} \approx 1/(2E_{\text{min}}) \approx 25000$, where $G_{\text{max}} \sim 12$, and $F = [1 + e^{-N_{\text{opt}} E_{\text{min}}}] / 2 = 0.82$. The optimal gain is achieved by 25000 entangled atoms distributed in $K_{\text{opt}} = N_{\text{opt}} / (Mn)_{\text{opt}} \approx 10$ clocks.

We presented and analyzed a protocol, capable of fully entangling ensembles of neutral atoms located in different atomic clocks. Local interactions are made robust by utilizing the strong interaction between Rydberg excitations, and non-local entanglement creation is made reliable with strong atom-light coupling, suppressed photon propagation errors and long atomic memory lifetimes. We showed that our scheme, in particular a realization with neutral Yb ensembles, is feasible and provides significant gain over non-entangled schemes even in the light of physical imperfections. Our results provide the first detailed proposal for a neutral atom clock network that can serve as a first prototype of the global quantum clock

network outlined in [6].

We are grateful to Kyle Beloy, Shimon Kolkowitz, Ronen Kroeze, Travis Nicholson, Thibault Peyronel, Alp Sipahigil, Jeff Thompson, and Leo Zhou for enlightening discussions. This work was supported by NSF, CUA, NIST, NASA, Simons Foundation, AFOSR MURI, ARL and NSSEFF fellowship.

SUPPLEMENTARY MATERIALS

Appendix A: Using the messenger atom

With proper optical control, we can entangle the ensembles by moving a single Rydberg atom to the vicinity of each ensemble sequentially, such that its blockade radius covers one of the clouds entirely. Starting from the state

$$|g\rangle^{nM}(|s\rangle + |r_2\rangle), \quad (\text{A1})$$

where the first nM ket stand for the state of all atoms in the M ensembles (each having n atoms), and the last one represents the state of the messenger atom. In a sequence, we imagine the messenger atom to be brought to the vicinity of each ensemble, and the pulse sequence $[\pi/\sqrt{N}]_{g,r1}, [pi]_{f,r1}$, creates an f excitation, conditioned on the state of the messenger atom. This plays out as follows

$$\rightarrow |g\rangle^{n(M-1)}(|1_f\rangle_1|s\rangle + |0\rangle_1|r_2\rangle) \quad (\text{A2})$$

$$\rightarrow |g\rangle^{n(M-2)}(|1_f\rangle_1|1_f\rangle_2|s\rangle + |0\rangle_1|0\rangle_2|r_2\rangle) \quad (\text{A3})$$

$$\vdots \quad (\text{A4})$$

$$\rightarrow (|1_f\rangle^M|s\rangle + |0\rangle^M|r_2\rangle), \quad (\text{A5})$$

which then only requires the messenger atom to be measured in the $|\pm\rangle = (|s\rangle \pm |r_2\rangle)$ basis, resulting in

$$\rightarrow |1_f\rangle^M \pm |0\rangle^M, \quad (\text{A6})$$

the required entangled state before the final GHZ extension step.

Disregarding the technical difficulties of trapping multiple atomic ensembles in the same vacuum chamber, this entangling method has a higher fidelity than the previous, photon-based, protocol, since it does not suffer from the errors affecting the photon emission, propagation and detection. We model the imperfections of this scheme by summing the error terms $\varepsilon_1 + \varepsilon_2 + \varepsilon_3$ only (from Eq. (C2), (C5), (C7)).

Appendix B: Overview of optimization

In section G, we show that the figure of merit, the precision gain with respect to non-entangled schemes, can

be written as

$$G(N, E) = \frac{\pi}{8} e^{-EN} \sqrt{\frac{N}{\log N}}, \quad (\text{B1})$$

where N is the total number of entangled atoms in the global GHZ state, and $E = E(n, \Omega)$ is the total error (contrast loss) divided by the total number of atoms. E depends on the number of atoms at a single clock, n , and the Rabi-frequency of the dressing field used for local entanglement growing.

We separate out the minimization of E (through finding the optimal n, Ω parameters), and the maximization of G (through finding the optimal N). In other words, we find

$$G_{\max} = \max_N G\left(N, \min_{n, \Omega} E\right). \quad (\text{B2})$$

This two-step procedure gives identical results to the full optimization,

$$G_{\max} = \max_{N, n, \Omega} G\left(N, E(n, \Omega)\right), \quad (\text{B3})$$

because both the maximum of G and the optimal value of N are monotonically decreasing functions of E , for large N (as can be seen from Eq. (B1)). We choose the two-step procedure because it is easier to carry out and interpret.

Appendix C: Local entangling errors

The initial GHZ state is never perfect due to a series of imperfections in the implementation. Here, we analyze the main errors responsible for lowering the initial fidelity $F_{\text{local}} = [1 + \exp(-\varepsilon_{\text{local}})]/2$ of the GHZ state of n atoms, created via the conditional dressing scheme, described in the main article. We assume the following errors to be independent and small, and we approximate $\varepsilon_{\text{local}}$ with the sum of the individual errors, $\sum_j \varepsilon_j$. We evaluate the errors for a 2D square lattice filled in a circular region and a 3D cubic lattice filled in a spherical region (both of radius R). Where there is a difference between the two cases, we give both results.

1. Imperfect blockade

If the blockade between the levels r_1 and r_2 , Δ_{12} , is not large enough, the population transfer $g \rightarrow f$ happens even if r_2 is populated by a single atom. Here, we analyze the effect of this imperfection.

Each pulse $\left[\frac{\pi}{\sqrt{n-j+1}}\right]_{g,r1}$, for $j = 1, 2, \dots, n$ excites an average population of $\sim n \left(\frac{\Omega}{2\Delta_{12}}\right)$ to the r_1 Rydberg

state even if it is detuned by Δ_{12} due to the interaction with the control atom being in r_2 state. There are n such pulses total, resulting in the error

$$\varepsilon_1 = \frac{n^2 \Omega^2}{4} \left\langle \frac{1}{\Delta_{12}^2} \right\rangle, \quad (\text{C1})$$

where the average is taken over every pair of atoms in the ensemble. After calculating this average for 2D and 3D spherical ensembles with uniform density, we obtain

$$\varepsilon_1 = \left(\frac{\hbar a^3 \Omega}{C_{12}^{(3)}} \right)^2 \times \begin{cases} 0.02818 n^5 & (2\text{D}) \\ 0.06079 n^4 & (3\text{D}) \end{cases}, \quad (\text{C2})$$

where $C_{12}^{(3)}$ is the dipole-dipole coefficient of the interaction between r_1 and r_2 , and a is the lattice constant of the square (cubic) lattice of the 2D (3D) ensemble.

2. Decaying Rydberg states

During the pulse sequence that induce the population transfer from g to f , the r_1 level is populated by an average of $1/2$ atoms. With constant Ω Rabi frequency, the times of the pulse j is $\frac{\pi}{\Omega\sqrt{j}}$. The total accumulated error during the pulse sequence due to decay or dephasing of r_1 Rydberg state is

$$\varepsilon_2^{(1)} = \frac{\gamma_1}{2} \frac{\pi}{\Omega} 2 \sum_{j=1}^n \frac{1}{\sqrt{j}} \approx \gamma \sqrt{n} \frac{2\pi}{\Omega} \quad (\text{C3})$$

where γ_1 is the total rate of loss (environment induced decay and dephasing) from the Rydberg level r_1 . The additional factor of 2 appears because both the $g \rightarrow r_1$ and $r_1 \rightarrow f$ transfers need to happen.

In the meantime, the r_2 level is populated by a single atom. The decay and dephasing of r_2 , which we assume to be happening with rate γ_2 causes error accumulation, which we approximate as

$$\varepsilon_2^{(2)} = \gamma_2 \frac{\pi}{\Omega} 2 \sum_{j=1}^n \frac{1}{\sqrt{j}} \approx \gamma \sqrt{n} \frac{4\pi}{\Omega}. \quad (\text{C4})$$

Although the two errors affect different components of the wavefunction, we use their sum as an upper bound of their effect:

$$\varepsilon_2 = \varepsilon_2^{(1)} + \varepsilon_2^{(2)} = 6\pi \sqrt{n} \frac{\gamma}{\Omega}. \quad (\text{C5})$$

3. Imperfect self-blockade

During the excitation of the Rydberg state r_1 , double excitations are mostly shifted out of resonance by Δ_{11} due to the strong van der Waals interaction between two r_1 atoms. The time average of the population in the state where one Rydberg atom is excited is $1/2$. The

collective Rabi frequency between the 1-Rydberg state and the 2-Rydberg state is $\sqrt{2(n-1)}\Omega$. This translates to an average population of $(n-1) \left(\frac{\Omega}{2\Delta_{11}} \right)$ during a single pulse. Since there are n such pulses during the population transfer from g to f , the total accumulated error is

$$\varepsilon_3 \approx \frac{n^2 \Omega^2}{4} \left\langle \frac{1}{\Delta_{11}^2} \right\rangle. \quad (\text{C6})$$

After evaluating the average over all pair in the 2D (3D) ensemble, we obtain

$$\varepsilon_3 = \left(\frac{\hbar a^6 \Omega}{C_{11}^{(6)}} \right)^2 \times \begin{cases} 0.01594 n^8 & (2\text{D}) \\ 0.05544 n^6 & (3\text{D}) \end{cases} \quad (\text{C7})$$

where $C_{11}^{(6)}$ is the van der Waals coefficient of the interaction between two r_1 atoms, and a is the lattice constant of the square (cubic) lattice of the 2D (3D) ensemble.

Appendix D: Non-local entangling errors

Our protocol requires $K-1$ links to be set up between K clocks. We denote the fidelity of a single connection by $F_{\text{non-local}} = [1 + \exp(-\varepsilon_{\text{non-local}})]/2$, and we approximate $\varepsilon_{\text{non-local}}$ with the sum of individual errors $\sum_i \varepsilon_i$, detailed below.

1. Imperfect blockade

When exciting a single collective excitations, imperfect self-blockade can result in leakage into double excited states. The probability of this can be exponentially reduced by applying a smooth driving pulse. E.g., in case of a Gaussian pulse of width τ , and area π , exciting the $g \rightarrow r_1$ transition is expected to be blocked when r_2 is populated, but it succeeds with probability P_{double} ,

$$P_{\text{double}} \approx \frac{\pi^2}{4} \exp \left[-\frac{(\Delta_{12}\tau)^2}{2} \right], \quad (\text{D1})$$

where $\Delta_{12} = C_{12}^{(3)}/(\hbar(2R)^3)$ is the minimal energy shift in the ensemble due to the interaction of two atoms, one in r_1 and one in r_2 . A detailed analysis of how different pulses affect the transition probability can be found in [40]. $P_{\text{double}} \ll 1$ requires

$$\tau \leq \frac{\sqrt{2}}{\Delta_{12}} = \begin{cases} 2n^{3/2} \frac{\hbar a^3}{C_{12}^{(3)}} & (2\text{D}) \\ 2.7 n \frac{\hbar a^3}{C_{12}^{(3)}} & (3\text{D}) \end{cases} \quad (\text{D2})$$

in order to be small compared to the other errors.

2. Rydberg state decay

The $g \rightarrow r_1$ transition is driven with a pulse of duration τ , during which the r_2 level has a single excitation, which

decays with rate γ_2 . The resulting error contribution, after all four photon pulses have been generated, is

$$\varepsilon_4 = 4\gamma_2\tau = \begin{cases} 8n^{3/2} \frac{\hbar a^3 \gamma_2}{C_{12}^{(3)}} & (2D) \\ 10.8 n \frac{\hbar a^3 \gamma_2}{C_{12}^{(3)}} & (3D) \end{cases} \quad (D3)$$

where we used the expressions for τ from Eq. (D2).

3. Photon propagation and detection errors

The pairs of photons can get lost in the fiber during propagation and the detection process (which is limited to 50% for time-resolving detectors, and 25% for non-time-resolving ones). The two-photon heralding, however, detects both of these errors. The remaining error comes from dark-counts of the detectors. This affects a single link with the error

$$\varepsilon_5 \approx 4\gamma_{\text{dark}}T_{\text{detect}} = \gamma_{\text{dark}} \frac{20}{n\gamma_e}, \quad (D4)$$

where γ_{dark} is the dark count rate of the detectors, T_{detect} (chosen such that a properly timed detector would have a chance to catch $1 - e^{-5} > 99\%$ of each photon) is the “open time” of the detector, and γ_e is the spontaneous emission lifetime of the $|e\rangle \rightarrow |f\rangle$ transitions. The factor of n is due to the collective enhancement of the said transition, and the factor of 4 is because four pulses are used in each connection.

4. Memory loss

During the creation step of each link, the state $|s\rangle$ is used as memory. On average, every link relies on one s qubit. The time it takes to attempt the creation of a link is $\sim 2L/c$, the time it takes for a light pulse to do a round-trip between two stations. During this time, quantum information is stored in qubit s , which is subject to decoherence happening at a rate γ_s . The infidelity of the link originating from this error is

$$\varepsilon_6 = 4 \frac{2L}{c} \gamma_s. \quad (D5)$$

State $|f\rangle$ is assumed to be a long-lived clock state, its decoherence rate is negligible.

5. Imperfect photon collection

Collective enhancement makes the excited atom in state $|e\rangle$ decay preferentially to $|g\rangle$, and emit a photon directly to the spatial mode \mathbf{k}_e , where \mathbf{k}_e is the spatial frequency of the collective mode e . In the implementation with Yb atoms (discussed in Section E), the decay channel to $|g\rangle$ has a close to unity branching ratio ($\zeta = 0.99$),

but due to the finite size of the ensemble, the photon collection efficiency is decreased. The probability of not capturing the emitted photon is

$$\varepsilon_7 \approx \frac{k_e^2 w^2}{3nf} = \begin{cases} \frac{k_e^2 a^2}{3\pi f}, & (2D) \\ \frac{k_e^2 a^2}{3n^{1/3} f} \left(\frac{3}{4\pi}\right)^{2/3}, & (3D) \end{cases} \quad (D6)$$

where w is the radius of the ensembles cross section perpendicular to \mathbf{k}_e , ($w = a(n/\pi)^{1/2}$ for 2D, and $w = a(3n/(4\pi))^{1/3}$ for 3D.), and $k_e = 2\pi/(1.4\mu\text{m})$, and $f \sim 100$ is the finesse of the cavity that we envision using.

Appendix E: Implementation with Yb

We imagine using the lower levels of neutral Yb for our protocol, $|g\rangle = |6s^2(^1S_0)\rangle$, $|f\rangle = |6s6p(^3P_0)\rangle$, $|s\rangle = |6s6p(^3P_2)\rangle$ and $|e\rangle = |6s6p(^1P_1)\rangle$, and two Rydberg levels $|r_1\rangle = |6s\tilde{n}p_{m=+1}(^1P_1)\rangle$ and $|r_2\rangle = |6s\tilde{n}s(^3S_1)\rangle$ with the same principle quantum number \tilde{n} . In the case of the 2D lattice, we set the quantization axis perpendicular to the plane in which the atoms reside, this way the dipole-dipole interaction between two atoms, one in $|r_2\rangle$ and the other in $|r_1\rangle$, depends only on their separation, $|\mathbf{r}_1 - \mathbf{r}_2|$. In the case of the 3D lattice, we rely on the overwhelming strength of the Rydberg interaction to produce reliable blockade even between atoms in different horizontal planes.

1. Rydberg lifetimes

We use the measured values from [41] for principle quantum numbers $\tilde{n} \sim 20 - 30$, and extrapolate the inverse lifetimes of the Rydberg states

$$\gamma_1 \approx \gamma_2 = \gamma = \frac{8.403 \times 10^8 \text{ s}^{-1}}{(\tilde{n} - 4.279)^3} \quad (E1)$$

where \tilde{n} is the principle quantum number of the Rydberg orbit. Although the measurement was carried out at 300 K, the contribution of the black body radiation (at $\tilde{n} \sim 20 - 30$) is negligible even at this temperature, and therefore our extrapolation accurately describes the effect of spontaneous emission on the lifetime. Cooling of the radiation environment will be necessary to reach the above lifetime at $\tilde{n} \sim 100$ and above. Furthermore, the photoionization rate in a trapping field with 10^4 W/cm^2 intensity is also more than one order of magnitude smaller.

2. Self-blockade, Δ_{11}

The long-range interaction between two r_1 atoms at a distance R is dominated by the van der Waals potential,

$$\Delta_{11}(R) = \frac{C_{11}^{(6)}}{\hbar R^6}, \quad (E2)$$

where $C_{11}^{(6)}$ strongly depends on the principle quantum number \tilde{n} . We use results from [42], and extrapolate the $C_{11}^{(6)}$ coefficient to high principle quantum numbers with the following formula,

$$C_{11}^{(6)} = (-0.116 + 0.0339\tilde{n})\tilde{n}^{11} \text{ a.u.} \quad (\text{E3})$$

where the a.u. stands for atomic units, $E_h a_0^6 = 9.573 \times 10^{-80} \text{ Jm}^6$, where E_h is the Hartree energy and a_0 is the Bohr radius.

3. Cross-blockade, Δ_{12}

The long-range interaction between an r_1 and an r_2 atoms at a distance R is dominated by the dipole-dipole interaction. We assume that the atoms are confined in the xy plane, and because the $6s\tilde{n}p_{m=+1}$ state is polarized in the z direction, the interaction strength is independent of the relative direction of one atom to the other.

$$\Delta_{12}(R) = \frac{C_{12}^{(3)}}{\hbar R^3}, \quad (\text{E4})$$

where $C_{12}^{(3)}$ depends strongly on the principle quantum number \tilde{n} . We use results from [42], and extrapolate the $C_{12}^{(3)}$ coefficient to high principle quantum numbers with the following formula,

$$C_{12}^{(3)} = (0.149 + 0.00077\tilde{n})\tilde{n}^4 \text{ a.u.} \quad (\text{E5})$$

where the a.u. stands for atomic units, $E_h a_0^3 = 6.460 \times 10^{-49} \text{ Jm}^3$.

4. Decay rates of lower levels

The decay rate of $|s\rangle = |6s6p, {}^3P_2\rangle$ is $\gamma_s = [14.5 \text{ s}]^{-1} = 0.069 \text{ s}^{-1}$. The decay rate of the excited state $|e\rangle = |6s6p, {}^1P_1\rangle$ is $\gamma_e = 1.8 \times 10^8 \text{ s}^{-1}$.

5. Photon channels

We assume that neighboring stations are $L < 10 \text{ km}$ apart from each other, we neglect fiber and coupling loss. We further assume that single photon detectors have a low dark count rate, i.e. $\gamma_{\text{dark}} \approx 10 \text{ s}^{-1}$.

Appendix F: Optimization

The total initial imperfections of a GHZ state with N atoms divided into K clocks, each enclosing M equal-sized ensembles (each of which contain n atoms) is

$$\varepsilon_{\text{tot}} = (K-1)\varepsilon_{\text{non-local}} + MK\varepsilon_{\text{local}} \quad (\text{F1})$$

$$\approx N \left(\frac{\varepsilon_{\text{local}}}{n} + \frac{\varepsilon_{\text{non-local}}}{Mn} \right) =: NE, \quad (\text{F2})$$

where the error contributions are $\varepsilon_{\text{local}} = \varepsilon_1 + \varepsilon_2 + \varepsilon_3$, and $\varepsilon_{\text{non-local}} = \varepsilon_4 + \varepsilon_5 + \varepsilon_6 + \varepsilon_7$, from Eq. (C2, C5, C7, D3, D4, D5 and D6).

It is clear that the larger M is, the smaller the error is, however nM (the number of atoms in a single clock) is limited by the current state of technology to $(nM)_{\text{opt}} \sim 2500$. Independently from the total atom number, N , there is an optimal ensemble size, n_{opt} , for which E (the total error per atom) is minimal. Below we find the optimal values of the parameters Ω , (the Rabi frequency the population transfer), and n (the size of the each ensemble) for fixed values of \tilde{n} (the principle quantum number of the Rydberg state) and $a = 275.75 \text{ nm}$.

Using the following dimensionless variables, $\omega = \Omega/\gamma$, $\delta_{11} = \frac{C_{11}^{(6)}}{\hbar a^6 \gamma}$ and $\delta_{12} = \frac{C_{12}^{(3)}}{\hbar a^3 \gamma}$, we can write the error per atom as $E := \sum_i e_i$, where the terms are $e_i = \varepsilon_i/n$ for $i = 1, 2, 3$ and $e_i = \varepsilon_i/(Mn)_{\text{opt}} = \varepsilon_i/2500$ for $i = 4, 5, 6, 7$,

$$e_1 = \left(\frac{\omega}{\delta_{12}} \right)^2 \times \begin{cases} 0.02818 n^4 & (2\text{D}) \\ 0.06079 n^3 & (3\text{D}) \end{cases} \quad (\text{F3})$$

$$e_2 = \frac{6\pi}{n^{1/2}\omega} \quad (\text{F4})$$

$$e_3 = \left(\frac{\omega}{\delta_{11}} \right)^2 \times \begin{cases} 0.01594 n^7 & (2\text{D}) \\ 0.05544 n^5 & (3\text{D}) \end{cases} \quad (\text{F5})$$

$$e_4 = \frac{1}{\delta_{12} \times 2500} \times \begin{cases} 8 n^{3/2} & (2\text{D}) \\ 10.8 n & (3\text{D}) \end{cases} \quad (\text{F6})$$

$$e_5 = 7.6 \times 10^{-5} \frac{1}{2500 \times n} \quad (\text{F7})$$

$$e_6 = 1.8 \times 10^{-5} / 2500 \quad (\text{F8})$$

$$e_7 = \frac{1.532}{3 \times 10^2 \times 2500} \times \begin{cases} \frac{1}{n^{1/3}} & (2\text{D}) \\ \frac{1}{n^{1/3}} \left(\frac{3}{4\pi} \right)^{2/3} & (3\text{D}) \end{cases} \quad (\text{F9})$$

1. Optimal parameters

We numerically minimized the sum, $E = \sum_i e_i$, by finding the optimal values of n for every $\tilde{n} \in [50, 150]$, for $\omega = 10^5$. The optimal number of atoms at a single ensemble n_{opt} are shown on Fig. 6.

The minimal error per atom E_{min} is shown on Fig. 7 as a function of \tilde{n} .

2. Comparison of error sources

We compare the contributions of the different error terms e_i to the total error per atom, $\sum_i e_i$, for $\tilde{n} = 120$. The different error terms contribute to the sum with amounts given in Table II and III.

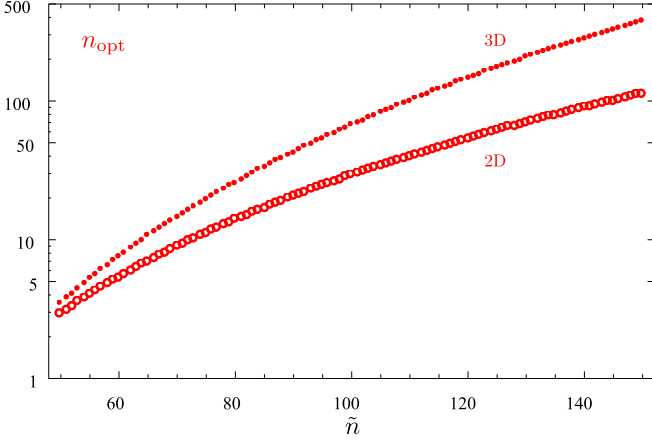


FIG. 6. The optimal number of atoms in a single ensemble n is plotted as a function of the principle quantum number of the Rydberg levels \tilde{n} , for the 2D and 3D setup.

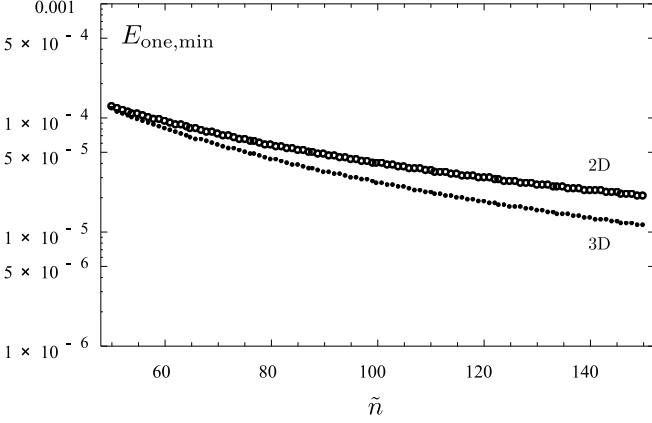


FIG. 7. The minimized error contribution of a single atom as a function of the principle quantum number of the Rydberg levels \tilde{n} , for the 2D and 3D setup.

Errors in 2D ensemble	error per atom	ratio in total
imperfect blockade (e_1)	3.2×10^{-6}	11%
Rydberg decay (e_2)	2.5×10^{-5}	87%
self-blockade (e_3)	$\sim 10^{-10}$	< 0.1%
r_2 decay (non-local) (e_4)	$\sim 10^{-11}$	< 0.1%
photon detection (e_5)	$\sim 10^{-12}$	< 0.1%
memory error (e_6)	$\sim 10^{-9}$	< 0.1%
photon collection (e_7)	6.5×10^{-7}	2%
total error per atom	3.0×10^{-5}	100%

TABLE II. The absolute and relative contribution of the different error sources to the total error per atom at $\tilde{n} = 120$, $\Omega = 10^5 \gamma$ and $n = n_{\text{opt}} = 54$.

Errors in 3D ensemble	error per atom	ratio in total
imperfect blockade (e_1)	2.6×10^{-6}	14%
Rydberg decay (e_2)	1.6×10^{-5}	86%
self-blockade (e_3)	$\sim 10^{-11}$	< 0.1%
r_2 decay (non-local) (e_4)	$\sim 10^{-11}$	< 0.1%
photon detection (e_5)	$\sim 10^{-12}$	< 0.1%
memory error (e_6)	$\sim 10^{-8}$	< 0.1%
photon collection (e_7)	$\sim 10^{-8}$	< 0.1%
total error per atom	1.8×10^{-5}	100%

TABLE III. The absolute and relative contribution of the different error sources to the total error per atom at $\tilde{n} = 120$, $\Omega = 10^5 \gamma$ and $n = n_{\text{opt}} = 146$.

Appendix G: Clock precision

1. Imperfect initialization

The precision of an atomic clock employing a GHZ state of N clock atoms is limited by the initial imperfect creation of the GHZ state described by the fidelity F_N or contrast $c = 2F_N - 1$. We assume that an imperfect creation of the GHZ state result in the density matrix

$$\rho_{\text{non-pure}} = c|\Psi\rangle\langle\Psi| + \frac{1-c}{2}(|0\rangle\langle 0| + |1\rangle\langle 1|), \quad (\text{G1})$$

where $|\Psi\rangle = \frac{|0\rangle + |1\rangle}{\sqrt{2}}$, $|0\rangle = |0\rangle^{\otimes N}$, $|1\rangle = |1\rangle^{\otimes N}$, and we assumed that only the relative phase between the two components of the GHZ state changes to an unknown value, but no relaxation happens.

2. Measurement

After the interrogation time, the two components of the GHZ state pick up a relative phase $N\phi$. $|\Psi\rangle \rightarrow |\Psi_\phi\rangle = [|0\rangle + e^{iN\phi}|1\rangle]/\sqrt{2}$. Performing a perfect single-atom $-\pi/2$ rotation around the y axis for all atoms transforms this into

$$|\Psi'_\phi\rangle = \frac{1}{\sqrt{2^{N+1}}} \sum_{\{q_j\}} \left[1 + (-1)^{\sum_j q_j} e^{iN\phi} \right] |q_1, q_2, \dots, q_N\rangle, \quad (\text{G2})$$

where $q_j \in \{0, 1\}$ stands for the state of atom j . After this, we measure every atom (in the z -basis). The probability of any resulting sequence, $\mathbf{q} = (q_1, q_2, \dots, q_N) \in \{0, 1\}^{\times N}$, is

$$\mathcal{P}(\mathbf{q}|\Psi'_\phi) = \frac{1}{2^{N+1}} \left[1 + (-1)^{\sum_j q_j} \cos(N\phi) \right], \quad (\text{G3})$$

and the probability of the parity, $p = (\sum_j q_j) \bmod 2$, is

$$\mathcal{P}(p|\Psi'_\phi) = \frac{1 + (-1)^p \cos(N\phi)}{2}, \quad p \in \{0, 1\}. \quad (\text{G4})$$

On the other hand, these probabilities are different when they are conditioned on being in the mixed part

of the density matrix.

$$\mathcal{P}(\mathbf{q}|\rho_{\text{mixed}}) = \frac{1}{2^N}, \quad \mathcal{P}(p|\rho_{\text{mixed}}) = \frac{1}{2} \quad (\text{G5})$$

$\forall \mathbf{q} \in \{0, 1\}^{\times N}$ and $\forall p \in \{0, 1\}$, where $\rho_{\text{mixed}} = [|\mathbf{0}\rangle\langle\mathbf{0}| + |\mathbf{1}\rangle\langle\mathbf{1}|]/2$.

The resulting total probability is the weighted sum of the two cases,

$$\mathcal{P}(p|\phi) = c\mathcal{P}(p|\Psi'_\phi) + (1-c)\mathcal{P}(p|\rho_{\text{mixed}}) \quad (\text{G6})$$

$$= \frac{1 + c(-1)^p \cos(N\phi)}{2}, \quad (\text{G7})$$

where $c = 2F_N - 1$ is the contrast of the interference fringes.

3. Fisher information

We rely on inferring the unknown phase ϕ , from a series of parity measurements, as described above. The information content (about ϕ) of a single measured value p is quantified by the Fisher information,

$$\mathcal{F}(\phi) = \sum_{p \in \{0,1\}} \mathcal{P}(p|\phi) \left[\ln \frac{d}{d\phi} \mathcal{P}(p|\phi) \right]^2 \quad (\text{G8})$$

$$= N^2 \frac{\sin^2(N\phi)}{1/c^2 - \cos^2(N\phi)}, \quad (\text{G9})$$

where the true value of the phase is ϕ . The average Fisher information is

$$\bar{\mathcal{F}} = \frac{1}{2\pi} \int_{-\pi}^{+\pi} d\phi \mathcal{F}(\phi), \quad (\text{G10})$$

which we can evaluate in the limit of $c \ll 1$,

$$\bar{\mathcal{F}} \approx \frac{1}{2\pi} \int d\phi c^2 \cos^2(N\phi) = \frac{N^2 c^2}{2}. \quad (\text{G11})$$

In the other limit, when $1-c \ll 1$, $F(\phi)$ is approximately c^2 everywhere, except near the points where $\sin(N\phi) = 0$. We approximate the dip at $\phi = 0$ with

$$\frac{\sin^2 x}{1/c^2 - \cos^2 x} \approx \frac{x^2}{\frac{1-c^2}{c^2} + x^2}, \quad \text{where } x = N\phi, \quad (\text{G12})$$

and the integral with

$$\frac{\bar{\mathcal{F}}}{N^2} \approx c^2 - \frac{2}{2\pi} \int_{-\pi}^{+\pi} dx \left(1 - \frac{x^2}{\frac{1-c^2}{c^2} + x^2} \right) \quad (\text{G13})$$

$$= c^2 - \frac{\sqrt{1-c^2}}{c} \approx 1 - \sqrt{2(1-c)}, \quad (\text{G14})$$

where we have used that F is periodic with period $2\pi/N$.

Using these two limits for the average Fisher information, we approximate it with

$$\bar{\mathcal{F}} \approx \begin{cases} N^2 c^2 / 2 & , \quad \text{if } c \leq 0.7, \\ N^2 \left(1 - \sqrt{2(1-c)} \right) & , \quad \text{if } 1-c > 0.7. \end{cases} \quad (\text{G15})$$

The quality of this approximation can be read off from Fig. 8

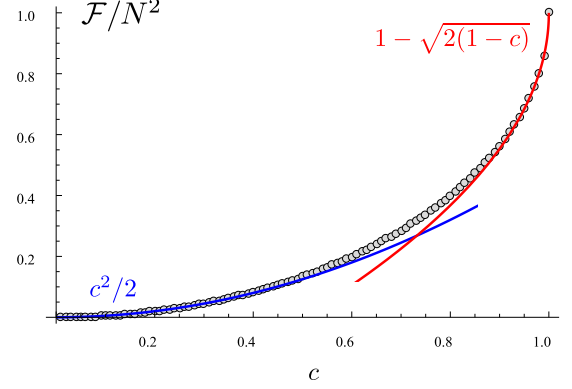


FIG. 8. Average Fisher information as a function of the contrast c (dots). It is well approximation by $c^2/2$ for $c < 0.6$ and by $1 - \sqrt{2(1-c)}$ for $c > 0.8$ (solid curves).

4. Cramér-Rao bound

The average Fisher information $\bar{\mathcal{F}}$ is a good measure of the posterior uncertainty of the phase ϕ , if the prior distribution of the phase has been previously narrowed down to a small enough interval such that its posterior is single peaked. In case of using the GHZ state, this requires a very narrow prior to start with: $\phi \in [-\pi/N, +\pi/N]$. In our previous work, we showed that this is possible by employing the atoms in a scheme using a series of cascaded GHZ states [7]. The Cramér-Rao bound on the expected deviation of the estimated ϕ from the true one implies

$$\Delta\phi = \sqrt{\langle (\phi_{\text{estimate}} - \phi_{\text{true}})^2 \rangle} \geq \left[\nu \bar{\mathcal{F}} \right]^{-1/2}, \quad (\text{G16})$$

where ν is the number of independent repetitions of the measurement. We are going to assume equality to simplify our analysis.

5. Allan deviation

The average fractional frequency uncertainty of an atomic clock (with central frequency ω_0), averaged over a long time period τ , is called Allan deviation [7],

$$\sigma = \frac{(\Delta\omega)_\tau}{\omega_0} \approx \frac{\Delta\phi_t/t}{\omega_0} \frac{1}{\sqrt{\tau/t}} \approx \frac{1}{\omega_0 \sqrt{\tau}} [\nu t \bar{\mathcal{F}}]^{-1/2} \quad (\text{G17})$$

where $(\Delta\omega)_\tau = \left| \frac{1}{\tau} \int d\tau' \omega(\tau') - \omega_0 \right|$ is the deviation of the average frequency over time τ , and $\Delta\phi_t$ is the average deviation of the measured phase (from the true one) in a single interrogation of length t . The $\sqrt{\tau}/t$ factor comes from the number of independent repetitions of the same, t -long, interrogation cycle.

In Ref. [6], we showed that σ can reach

$$\sigma_{\text{ent}} \approx \frac{1}{\omega_0 \tau} \frac{8}{\pi} \frac{\sqrt{\log N}}{N}, \quad (\text{G18})$$

if $\tau < \gamma_{\text{at}}^{-1}/N$, the reduced atomic coherence time, and if the contrast is perfect, ($c = 1$). Using the approximation for $\bar{\mathcal{F}} \approx N^2 c^2/2$, and the fact that $\sigma \propto [\bar{\mathcal{F}}]^{-1/2} \propto c^{-1}$, we can augment this result with a c -dependence, and express the Allan deviation in the presence of imperfections as

$$\sigma_{\text{ent}}^{(\text{imperfect})} = \sigma_{\text{ent}}/c = \frac{1}{c\omega_0 \tau} \frac{8}{\pi} \frac{\sqrt{\log N}}{N}. \quad (\text{G19})$$

6. Comparison to non-entangled interrogation

Using the same number of atoms, N , we can arrange a measurement without using any entanglement. This results in the Allan deviation of

$$\sigma_{\text{non-ent}}(\tau) \approx \frac{1}{\omega_0 \tau \sqrt{N}}, \quad \text{if } \tau < 1/\gamma_{\text{LO}}, \quad (\text{G20})$$

where γ_{LO}^{-1} is the laser coherence time. This, representing the standard quantum limit (SQL), is expected to be larger than the Allan deviation corresponding to the GHZ state scheme, which is almost at the Heisenberg limit. The precision gain of the GHZ scheme over the non-entangled one is

$$G = \frac{\sigma_{\text{non-ent}}}{\sigma_{\text{ent}}/c} = (2F_N - 1) \frac{\pi}{8} \sqrt{\frac{N}{\log N}}. \quad (\text{G21})$$

Since the fidelity F_N decreases with increasing N , there exist an optimal N_{opt} , for which the gain G is maximal.

7. Optimal clock network size

If each clock runs with the optimal setup (n_{opt}), then the total error per atom, E , is minimal, and the total fidelity can be written as $F_N = [1 + e^{-E_{\text{min}} N}]/2$. Plugging this into Eq. (G21) gives

$$G = e^{-E_{\text{min}} N} \frac{\pi}{8} \sqrt{\frac{N}{\log N}}, \quad (\text{G22})$$

which takes its maximum at $N = N_{\text{max}} \approx \frac{1}{2E_{\text{min}}}$, giving $G_{\text{max}} \approx \frac{\pi}{8} \left[E_{\text{min}} \log \left(\frac{1}{2E_{\text{min}}} \right) \right]^{-1/2}$. In the meantime the

number of atoms at a single clock is ~ 2500 . As a result the optimal number of clocks becomes

$$K_{\text{opt}} \sim \frac{N_{\text{max}}}{2500}. \quad (\text{G23})$$

On Fig. 9, we plot N_{max} , n_{opt} , and K_{opt} as a function of the principle quantum number of the Rydberg states \tilde{n} . For $\tilde{n} = 120$, we find $N_{\text{max}} \approx 15000$ (2D) and \approx

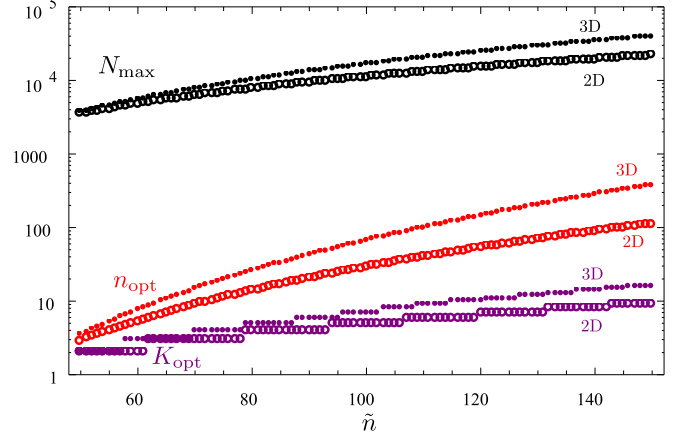


FIG. 9. The optimal total number of entangled atoms in the network N_{max} and the number of atoms at a single clock n_{opt} as a function of the principle quantum number \tilde{n} . The thin dotted lines show the multiples of n_{opt} . The optimal number of clocks, $K_{\text{opt}} \sim N_{\text{max}}/2500$ is written on the corresponding regions of \tilde{n} , for the 2D and 3D setup.

25000 (3D). Using the n_{opt} values from before (≈ 50 and ≈ 150), we find $K_{\text{opt}} \sim 6$ and ~ 10 , for 2D and 3D, respectively.

With the optimal architecture, we can plot the maximal gain G_{max} (compared to the non-entangled scheme using the same number of atoms) as a function of principle quantum number \tilde{n} . This is shown on Fig. 10. For $\tilde{n} = 120$, the gain is $G_{\text{max}} = 10$ (2D) and 12 (3D).

Appendix H: Calculating $\langle 1/\Delta_{12}^2 \rangle$

Here, we calculate the average of

$$\frac{1}{\Delta_{12}^2} = \left(\frac{\hbar}{C_{12}^{(3)}} \right)^2 |\mathbf{r}_1 - \mathbf{r}_2|^6 \quad (\text{H1})$$

for all (j, k) pairs in an ensemble of n atoms, trapped in a (square or cubic) lattice with periodicity a , uniformly filling a circular 2D (spherical 3D) region of radius R .

Averaging over the cloud of atoms, can be approximated by the following integral

$$\left\langle \frac{1}{\Delta_{12}^2} \right\rangle \approx \left(\frac{\hbar}{C_{12}^{(3)}} \right)^2 \underbrace{\frac{1}{V^2} \int_V d^n \mathbf{r}_j \int_V d^n \mathbf{r}_k |\mathbf{r}_j - \mathbf{r}_k|^6}_{R^6 I} \quad (\text{H2})$$

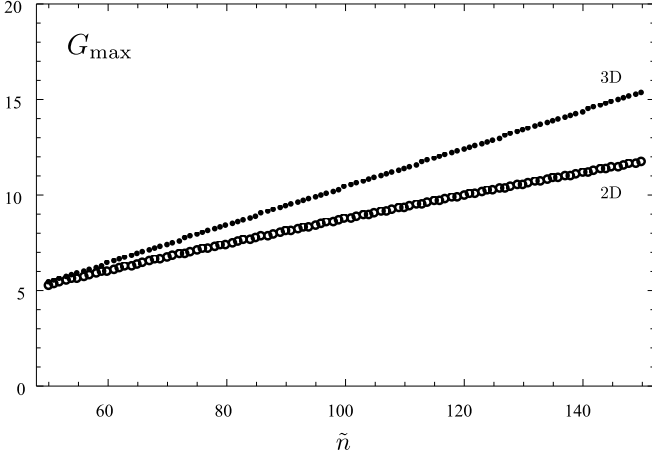


FIG. 10. Maximal gain over the non-entangled scheme provided by the optimal entangled clock network architecture as a function of principle quantum number of the Rydberg states \tilde{n} , for the 2D and 3D setup.

where $\eta = 2, 3$, V is the filled region, of radius R , in a (2D or 3D) lattice.

We introduce new variables $x = |\mathbf{r}_j - \mathbf{r}_k|$, $r = |\mathbf{r}_j|$, and use the circular symmetry of the cloud and the spherical symmetry of the interaction, to turn the integrals into one dimensional ones.

$$R^6 I_{2D} = \frac{1}{(\pi R^2)^2} \int_0^R dr 2\pi r \int_0^{2R} dx S_R(r, x) x^6, \quad (\text{H3})$$

$$R^6 I_{2D} = \frac{1}{(4\pi R^3/3)^2} \int_0^R dr 4\pi r^2 \int_0^{2R} dx A_R(r, x) x^6, \quad (\text{H4})$$

where the weighting factor $S_R(r, x)$ is the length of the segment of a circle of radius x , centered at r distance from the origin that lies inside the 2D cloud of radius R . (See Fig. 11). It can be written as

$$S_R(r, x) = \begin{cases} 2\pi x & , \text{ if } x < R - r \\ 0 & , \text{ if } R + r < x \\ 2x \arccos\left(\frac{x^2 + r^2 - R^2}{2xr}\right) & , \text{ otherwise} \end{cases} \quad (\text{H5})$$

Similarly, $A_R(r, x)$ is the area of a spherical surface or radius x centered r distance from the center of the 3D cloud located inside the cloud. It can be written as

$$A_R(r, x) = \begin{cases} 4\pi x^2 & , \text{ if } x < R - r \\ 0 & , \text{ if } R + r < x \\ \pi \frac{x}{r} [R^2 - (x - r)^2] & , \text{ otherwise} \end{cases} \quad (\text{H6})$$

Using the explicit expressions of Eq. (H5) and (H6), we

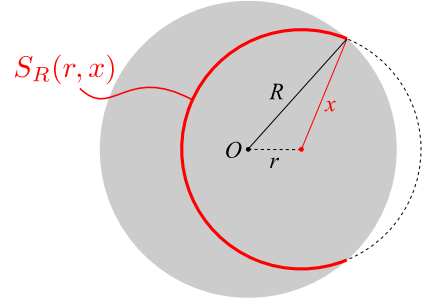


FIG. 11. The length of the circle segment of radius x lying inside the cloud of radius R , $S_R(r, x)$, is between 0 and $2\pi x$ for $R - r < x < R + r$, where r is the separation between the centers.

can write

$$I_{2D} = 4 \int_0^1 d\rho \rho \int_0^{1-\rho} d\xi \xi^7 + \quad (\text{H7})$$

$$+ 4 \int_0^1 d\rho \rho \int_{1-\rho}^{1+\rho} d\xi \frac{1}{\pi} \xi^7 \arccos\left(\frac{\xi^2 + \rho^2 - 1}{2\rho\xi}\right) \quad (\text{H8})$$

$$I_{3D} = 9 \int_0^1 d\rho \rho^2 \int_0^{1-\rho} d\xi \xi^8 + \quad (\text{H9})$$

$$+ 9 \int_0^1 d\rho \rho^2 \int_{1-\rho}^{1+\rho} d\xi \frac{1}{4} \frac{\xi^7}{\rho} [1 - (\xi - \rho)^2], \quad (\text{H10})$$

which we numerically evaluate and find $I_{2D} = 3.5$, and $I_{3D} = 4.27$.

Using that $\pi R^2 = na^2$ (in 2D) and $4\pi R^3/3 = na^3$ (in 3D), we can obtain the expressions in Eq. (C2).

Appendix I: Calculating $\langle 1/\Delta_{11}^2 \rangle$

Following the same line of thoughts as in the previous section, we can write the average as

$$\left\langle \frac{1}{\Delta_{11}^2} \right\rangle \approx \left(\frac{\hbar}{C_{11}^{(6)}} \right)^2 \underbrace{\frac{1}{V^2} \int_V d^n \mathbf{r}_j \int_V d^n \mathbf{r}_k |\mathbf{r}_j - \mathbf{r}_k|^{12}}_{R^{12} J} \frac{1}{V^2}. \quad (\text{I1})$$

The integral J can be evaluated following the same methods as in the previous section, and we obtain $J_{2D} = 61.29$, $J_{3D} = 68.26$.

Using that $\pi R^2 = na^2$ (in 2D) and $4\pi R^3/3 = na^3$ (in 3D), we can obtain the expressions in Eq. (C7).

[1] A. D. Ludlow and J. Ye, *Comptes Rendus Physique* **16**, 499 (2015).

[2] N. Hinkley, J. A. Sherman, N. B. Phillips, M. Schioppo,

- N. D. Lemke, K. Beloy, M. Pizzocaro, C. W. Oates, and A. D. Ludlow, *Science* **341**, 1215 (2013).
- [3] B. J. Bloom, T. L. Nicholson, J. R. Williams, S. L. Campbell, M. Bishof, X. Zhang, W. Zhang, S. L. Bromley, and J. Ye, *Nature* **506**, 71 (2014).
- [4] T. Nicholson, S. Campbell, R. Hutson, G. Marti, B. Bloom, R. McNally, W. Zhang, M. Barrett, M. Safronova, G. Strouse, W. Tew, and J. Ye, *Nature Communications* **6**, 6896 (2015).
- [5] A. Derevianko and M. Pospelov, *Nature Physics* **10**, 933 (2014).
- [6] P. Kómár, E. M. Kessler, M. Bishof, L. Jiang, A. S. Sørensen, J. Ye, and M. D. Lukin, *Nature Physics* **10**, 582 (2014).
- [7] E. M. Kessler, P. Kómár, M. Bishof, L. Jiang, A. S. Sørensen, J. Ye, and M. D. Lukin, *Phys. Rev. Lett.* **112**, 190403 (2014).
- [8] D. W. Berry, B. L. Higgins, S. D. Bartlett, M. W. Mitchell, G. J. Pryde, and H. M. Wiseman, *Phys. Rev. A* **80**, 052114 (2009).
- [9] M. J. W. Hall, D. W. Berry, M. Zwierz, and H. M. Wiseman, *Phys. Rev. A* **85**, 041802 (2012).
- [10] O. Hosten, N. J. Engelsen, R. Krishnakumar, and M. A. Kasevich, *Nature* **529**, 505 (2016).
- [11] N. Sangouard, C. Simon, H. de Riedmatten, and N. Gisin, *Rev. Mod. Phys.* **83**, 33 (2011).
- [12] A. Sørensen and K. Mølmer, *Phys. Rev. Lett.* **82**, 1971 (1999).
- [13] M. Saffman, T. G. Walker, and K. Mølmer, *Rev. Mod. Phys.* **82**, 2313 (2010).
- [14] Y. O. Dudin and A. Kuzmich, *Science* **336**, 887 (2012).
- [15] Y. O. Dudin, A. G. Radnaev, R. Zhao, J. Z. Blumoff, T. A. B. Kennedy, and A. Kuzmich, *Phys. Rev. Lett.* **105**, 260502 (2010).
- [16] M. Ebert, M. Kwon, T. G. Walker, and M. Saffman, *Phys. Rev. Lett.* **115**, 093601 (2015).
- [17] M. D. Lukin, M. Fleischhauer, R. Cote, L. M. Duan, D. Jaksch, J. I. Cirac, and P. Zoller, *Phys. Rev. Lett.* **87**, 037901 (2001).
- [18] M. Müller, I. Lesanovsky, H. Weimer, H. P. Büchler, and P. Zoller, *Phys. Rev. Lett.* **102**, 170502 (2009).
- [19] B. Zhao, M. Müller, K. Hammerer, and P. Zoller, *Phys. Rev. A* **81**, 052329 (2010).
- [20] Y. Han, B. He, K. Heshami, C.-Z. Li, and C. Simon, *Phys. Rev. A* **81**, 052311 (2010).
- [21] M. H. Goerz, E. J. Halperin, J. M. Aytac, C. P. Koch, and K. B. Whaley, *Phys. Rev. A* **90**, 032329 (2014).
- [22] Y.-A. Chen, X.-H. Bao, Z.-S. Yuan, S. Chen, B. Zhao, and J.-W. Pan, *Phys. Rev. Lett.* **104**, 043601 (2010).
- [23] F. Bariani, Y. O. Dudin, T. A. B. Kennedy, and A. Kuzmich, *Phys. Rev. Lett.* **108**, 030501 (2012).
- [24] O. Firstenberg, T. Peyronel, Q.-Y. Liang, A. V. Gorshkov, M. D. Lukin, and V. Vuletić, *Nature* **502**, 71 (2013).
- [25] M. Antezza, C. Braggio, G. Carugno, A. Noto, R. Pasante, L. Rizzuto, G. Ruoso, and S. Spagnolo, *Phys. Rev. Lett.* **113**, 023601 (2014).
- [26] T. M. Weber, M. Hönig, T. Niederprüm, T. Manthey, O. Thomas, V. Guarrera, M. Fleischhauer, G. Barontini, and H. Ott, *Nature Physics* **11**, 157 (2015).
- [27] T. Topcu and A. Derevianko, *Phys. Rev. A* **88**, 043407 (2013).
- [28] I. I. Beterov, M. Saffman, E. A. Yakshina, V. P. Zhukov, D. B. Tretyakov, V. M. Entin, I. I. Ryabtsev, C. W. Mansell, C. McCormick, S. Bergamini, and M. P. Fedoruk, *Phys. Rev. A* **88**, 010303 (2013).
- [29] T. Topcu and A. Derevianko, *Phys. Rev. A* **89**, 023411 (2014).
- [30] L. Li, Y. O. Dudin, and A. Kuzmich, *Nature* **498**, 466 (2013).
- [31] L. M. Duan, M. D. Lukin, J. I. Cirac, and P. Zoller, *Nature* **414**, 413 (2001).
- [32] T. Honjo, H. Takesue, H. Kamada, Y. Nishida, O. Tadanaga, M. Asobe, and K. Inoue, *Optics Express* **15**, 13957 (2007).
- [33] A. Rubenok, J. A. Slater, P. Chan, I. Lucio-Martinez, and W. Tittel, *Phys. Rev. Lett.* **111**, 130501 (2013).
- [34] M. Lukin, *Rev. Mod. Phys.* **75**, 457 (2003).
- [35] D. Shwa, R. D. Cohen, A. Retzker, and N. Katz, *Phys. Rev. A* **88**, 063844 (2013).
- [36] M. Saffman and K. Mølmer, *Phys. Rev. Lett.* **102**, 240502 (2009).
- [37] H. Weimer, M. Müller, I. Lesanovsky, P. Zoller, and H. P. Büchler, *Nature Physics* **6**, 382 (2010).
- [38] A. Sørensen, L.-M. Duan, J. I. Cirac, and P. Zoller, *Nature* **409**, 63 (2000).
- [39] T. G. Tiecke, J. D. Thompson, N. P. de Leon, L. R. Liu, V. Vuletić, and M. D. Lukin, *Nature* **508**, 241 (2014).
- [40] C. W. S. Conover, *Phys. Rev. A* **84**, 1 (2011).
- [41] D.-W. Fang, W.-J. Xie, Y. Zhang, X. Hu, and Y.-Y. Liu, *Journal of Quantitative Spectroscopy and Radiative Transfer* **69**, 469473 (2001).
- [42] A. D. Turker Topcu, arXiv:1505.07152 (2015).